

Article

Thermosensitive Behavior Defines the Features of Poly(N-isopropylacrylamide)/Magnetite Nanoparticles for Cancer Management

Ionut-Cristian Radu ¹, Andreea-Cristina Ion Mirica ¹, Ariana Hudita ², Eugenia Tanasa ³, Horia Iovu ¹, Catalin Zaharia ^{1,*} and Bianca Galateanu ²

¹ Advanced Polymer Materials Group, Faculty of Chemical Engineering and Biotechnology, University Politehnica of Bucharest, 1-7 Gh. Polizu Street, RO-011061 Bucharest, Romania

² Department of Biochemistry and Molecular Biology, University of Bucharest, 91-95 Splaiul Independentei Street, RO-050095 Bucharest, Romania

³ Faculty of Applied Sciences, Department of Physics, University Politehnica of Bucharest, 313 Splaiul Independentei, RO-060042 Bucharest, Romania

* Correspondence: zaharia.catalin@gmail.com; Tel.: +40-727694492

Abstract: This paper reports the preparation and characterization of thermosensitive poly(N-isopropylacrylamide) (PNIPAM)/magnetite nanoparticles in various conditions. The nanoprecipitation conditions address the impact of the temperature on PNIPAM/magnetite nanoparticle features due to the thermosensitive character of PNIPAM. Hybrid nanoparticles with desired features (size, size distribution, agglomeration, and release profile) are prepared by nanoprecipitation in non-solvent (acetone) at various temperatures. These nanoparticles are targeted as nanocarriers to deliver doxorubicin in breast cancer cells. Therefore, three temperatures, below the LCST (lower critical solution temperature), around the LCST, and above the LCST, were chosen as the main parameters within nanoprecipitation. Besides temperature, another major parameter drives the nanoparticles' features: polymer solution concentration. In this regard, two variable parameters were used to study the characteristics of developed hybrid nanoparticles. After preparation, the hybrid nanoparticles were subjected to morphological and size distribution investigation by SEM and DLS. The doxorubicin loading and release measurements were also performed to reveal the behavior of the nanoparticles. Finally, the unloaded and loaded hybrid nanoparticles were biologically assessed within a cancer cells line (MCF7) in terms of biocompatibility, cancer cell viability, and cell morphology.

Keywords: PNIPAM; magnetite; nanoparticles; doxorubicin; breast cancer; drug delivery



Citation: Radu, I.-C.; Mirica, A.-C.I.; Hudita, A.; Tanasa, E.; Iovu, H.; Zaharia, C.; Galateanu, B. Thermosensitive Behavior Defines the Features of Poly(N-isopropylacrylamide)/Magnetite Nanoparticles for Cancer Management. *Appl. Sci.* **2023**, *13*, 4870. <https://doi.org/10.3390/app13084870>

Academic Editors: Christophe A. Serra and Daniela Giacomazza

Received: 24 February 2023

Revised: 27 March 2023

Accepted: 11 April 2023

Published: 13 April 2023



Copyright: © 2023 by the authors. Licensee MDPI, Basel, Switzerland. This article is an open access article distributed under the terms and conditions of the Creative Commons Attribution (CC BY) license (<https://creativecommons.org/licenses/by/4.0/>).

1. Introduction

Breast cancer is now the world's most prevalent cancer, according to statistics from the International Agency for Research on Cancer (IARC) [1–4]. The experts at the World Health Organization (WHO) revealed that 2.3 million women worldwide were diagnosed with breast cancer in 2020, and 685,000 died from it. Nowadays, 1 in 5 individuals around the world will develop one type of cancer in their lifetime [5–8]. Among them, breast cancer is a major public health problem in both developed and developing countries. The high mortality rate caused by breast cancer is due to its high rate of metastasis [6,9–12]. Conventional treatment consists of surgery and radiation therapy. In order to reduce the risk of metastasis, systemic therapy is recommended. Doxorubicin (DOX) belongs to the anthracycline family of antibiotics. Since its introduction in the early 1970s, doxorubicin has been generally considered the leading dynamic chemotherapeutic agent in the treatment of metastatic breast cancer [13]. However, DOX has several adverse effects due to its lack of selectivity with subsequent treatment failure. Furthermore, DOX has been reported to cause cardiotoxicity, acute nausea, vomiting, alopecia, stomatitis, or reactions [14–16].

The development of drug delivery systems has been employed to overcome several major issues of conventional systems. Thus, the lack of drug solubility, the targeted control of drug release, or increasing the circulating time are several main issues to be addressed. In addition, the toxicity should be reduced, or the immunogenicity minimized [17–19]. This fact is highly associated with non-selective or non-specific damage to healthy tissue [20,21]. Appropriate drug delivery is a key component to achieving an efficient drug recovery response. Recently, nanotechnology has been considered a powerful tool for creating carriers for specific molecules. Its role is to improve the stability, bioavailability, and pharmacokinetic profile of drugs and reduce their toxicity [22,23]. Nanocarriers and innovative formulations play a tremendous role in enhancing the drug's bioavailability and healing potential. This fact ensures the drug availability at the target site [24]. However, nanocarriers find numerous issues generated by the tumor microenvironment, such as acidity, hypoxia, abnormal temperature, or protein/enzyme levels. Therefore, these major issues can be managed by tailoring the physical and chemical properties of ongoing delivery systems [20,25]. In comparison to healthy tissue, tumor tissue exhibits a higher temperature, which represents a way to control the drug release by an external heating source [26,27]. The presence of inorganic nanoparticles besides the polymeric thermo-sensitive shell is beneficial. This will ensure a higher capacity to respond to external heating sources, reaching the required temperature [28–30].

Poly(N-isopropylacrylamide) (PNIPAM) is a thermo-sensitive water-soluble polymer that has been used to incorporate and release certain types of chemotherapeutic drugs. Thus, PNIPAM is part of a class of environmentally responsive biomaterials able to manifest changes in concordance with environmental stimuli (light, pH, ions, temperature, electric field, etc.) [31–34]. PNIPAM chains undergo conformational transitions in an aqueous solution in response to temperature. The lower critical solution temperature (LCST) of 32–34 °C for this “smart polymer” has made it useful for various applications such as valves and sensors, cell culture media, membranes, and drug delivery systems [35–38]. Numerous PNIPAM nanocarrier systems have been developed as candidates for use in biomedical applications [39–43]. The combined assembly of stimuli-responsive polymers with inorganic magnetic nanoparticles could exhibit properties for controlled delivery of doxorubicin into biological targets. With the inclusion of magnetic nanoparticles, the delivery system responds to an external magnetic field, enhancing transport activity. Moreover, hybrid systems containing magnetic NPs reduce tumor volume by magnetic hyperthermia when an alternating magnetic field is applied [44,45].

This study reports the development of poly(N-isopropylacrylamide)-magnetite (Fe_3O_4) smart nanoparticles for breast cancer therapy. The research reveals the influence of the main process parameters on the nanoparticle characteristics and release behavior as an optimization approach. An *in vitro* investigation of the drug release mechanism is presented along with the morphology (SEM) and particle size (DLS). Thus, we report the effect of the nanoprecipitation temperature on nanoparticle size, size distribution, and release behavior. This approach can be very helpful in optimizing an appropriate protocol to further prepare the polymeric nanocarriers.

2. Materials and Methods

2.1. Materials

The monomer, N-isopropylacrylamide (NIPAM) and all other used reagents, potassium phosphate (ACS reagent, $\geq 98\%$), potassium persulfate (KP), sodium hydroxide (anhydrous pellets, reagent grade, $\geq 98\%$), doxorubicin (HPLC, reagent grade 98–102%), acetone (ACS reagent, $\geq 99.5\%$), ferrous sulfate heptahydrate, iron chloride, and ammonium hydroxide were provided by Sigma-Aldrich (3050 SPRUCE Street, St. Louis, MO, USA). Magnetite nanoparticles (Fe_3O_4 NPs) were prepared by co-precipitation [17]. Briefly, the magnetic nanoparticles were synthesized starting from iron chloride (FeCl_3), ferrous sulfate heptahydrate ($\text{FeSO}_4 \cdot 7\text{H}_2\text{O}$), and ammonium hydroxide (NH_4OH). The iron chloride was water dissolved until a clear solution was obtained. The solution was added to the ferrous

sulfate under magnetic stirring. The mixture was then added to an ammonium hydroxide aqueous solution. The nanoparticles were separated and washed several times with ethanol and distilled water until a neutral pH was reached. Finally, the magnetic nanoparticles were dried at 60 °C for 12 h.

2.2. Methods

2.2.1. Preparation of PNIPAM/Magnetite Nanoparticles

PNIPAM is synthesized by free-radical polymerization in aqueous solution using NIPAM monomer and an initiator to trigger the reaction at 60 °C. Briefly, the monomer was dissolved in water (5%), and after the complete dissolution of the monomer, the solution was purged by bubbling nitrogen for 20 min. After that, the initiator KP (5×10^{-3} mol/mol) was added to the solution, and the reaction vessel was kept at constant temperature for 18 h. The obtained PNIPAM was dialyzed against distilled water to remove the unreacted monomer. Furthermore, the polymer was dried at 60 °C for 24 h. Next, PNIPAM aqueous solutions with various concentrations were prepared (Table 1) by dissolution into phosphate-buffered saline solution (pH 7.45) at room temperature. The magnetite nanoparticles were also dispersed in PBS by sonication. Polymer solution was added dropwise in a water-miscible organic solvent, acetone, under high stirring to prepare the PNIPAM/magnetite nanoparticles. The nanoprecipitation procedure involved the nanoparticles assembling at the contact with the non-solvent phase (acetone). The nanoprecipitation was performed at three different temperatures for non-solvent phase (30, 34, and 38 °C) to show the influence of the temperature sensitive PNIPAM behavior on the nanoparticle's characteristics.

Table 1. Composition of PNIPAM/magnetite nanoparticles.

Sample Name	PNIPAM Concentration (%, w/v)	Drug Content (%, w/w)	Magnetite Concentration	Solution/Non-Solvent Phase Ratio (v/v)
PNIPAM 0.25%	0.25			
PNIPAM 0.5%	0.5			
PNIPAM 1%	1	5	0.5% (w/w: magnetite/PNIPAM	10:90 (v/v: PNIPAM solution/acetone
PNIPAM 2%	2			
PNIPAM 4%	4			

The drug-loaded nanoparticles were obtained by encapsulation of the anti-cancer drug, doxorubicin. Briefly, the doxorubicin was dissolved in PNIPAM aqueous solutions with different concentrations (Table 1). The PNIPAM/drug aqueous solution was nano precipitated according to the above procedure. The drug-loaded nanoparticles were recovered by centrifugation (9000 rpm) and oven-dried at 50 °C. The dried drug-loaded nanoparticles were further used for drug release analysis (all samples) and biological assessment (only sample prepared at 34 °C).

2.2.2. Characterization of Magnetite Nanoparticles by X-ray Diffraction (XRD) and Transmission Electron Microscopy (TEM)

X-ray diffraction (XRD) spectra for synthesized magnetite nanoparticles were registered on a PANalytical X'PERT MPD X-ray Diffractometer in the range $2\theta = 10\text{--}80$. An X-ray beam characteristic to Cu K α radiation was used ($\lambda = 1.5418$ Å). Geometrical evaluation (size and shape), including the crystalline structure of magnetic nanoparticles, was investigated by high-resolution transmission electron microscopy (HR-TEM) using a TECNAI F30 G2 S-TWIN microscope operated at 300 kV with Energy Dispersive X-ray Analysis (EDAX) facility.

2.2.3. Morphological and Particle Size Measurements (SEM, DLS)

The size and morphology of the PNIPAM/magnetite nanoparticles were investigated by Scanning Electron Microscopy (SEM) using a Quanta Inspect F50, with a field emission

gun (FEG) having 1.2 nm resolution and an Energy Dispersive X-ray Spectrometer (EDXS) having 133 eV resolution at MnKa. Prior to analysis, the samples were gold coated.

The size distribution of the nanoparticles was evaluated by dynamic light scattering in a static domain using a Malvern Zetasizer Nano instrument (UK). The experiment was carried out using glass cuvettes with square apertures.

2.2.4. Drug Release Behavior

In vitro drug release behavior of doxorubicin-loaded PNIPAM/magnetite nanoparticles was investigated at 7.45 pH and 37 °C. Briefly, 5 mL of doxorubicin-loaded nanoparticles in phosphate-buffered saline solution (PBS, pH 7.45) was placed in a tubular cellulose membrane, followed by immersion in flasks with a fixed volume (35 mL). The flasks were further incubated in an orbital mixer (Benchmark Scientific, Sayreville, NJ, USA) at 400 rpm, and 37.0 ± 0.5 °C. A total of 5 mL of PBS dialysate was collected at predetermined time intervals and then investigated by UV–VIS spectroscopy (SHIMADZU UV-3600 instrument). To maintain a constant volume, after each collection, 5 mL of fresh PBS was added to every flask. Release and encapsulation efficiencies were computed as follows (Equations (1) and (2)):

$$\text{RE (\%)} = \frac{\text{amount of released DOX}}{\text{amount of the loaded DOX}} \times 100 \quad (1)$$

$$\text{EE (\%)} = \frac{\text{amount of the loaded DOX} - \text{amount of unloaded DOX}}{\text{amount of the loaded DOX}} \times 100 \quad (2)$$

2.2.5. In Vitro Biological Investigation on Free and Doxorubicin-Loaded PNIPAM/Magnetite Nanoparticles Cell Culture Model

Pristine and doxorubicin-loaded PNIPAM (0.25%)/magnetite NPs were subjected to in vitro biological evaluation in terms of determining their efficacy on cancer cells (MCF7 human breast adenocarcinoma cell line, ATCC). In this view, the cells were propagated in standard conditions of culture (37 °C, humidified atmosphere, and 5% CO₂) in complete culture medium (DMEM supplemented with 10% Fetal Bovine Serum (FBS) and 1% penicillin-streptomycin mixture).

MTT Assay

To determine the NPs' working dose (IC₅₀-inhibitory concentration 50), MCF7 cells were seeded in flat bottom 96-well plates at an initial cell density of 104 cells/cm² and treated after 24 h with the following dilutions of pristine and DOX-loaded PNIPAM/mag NPs: 25 mg/mL, 20 mg/mL, 15 mg/mL, 10 mg/mL, 7.5 mg/mL, 5 mg/mL, 1 mg/mL, 500 µg/mL, 250 µg/mL, 100 µg/mL, and 50 µg/mL. The treatments were kept in contact with the cells for 24 h, and then the monolayers were washed and incubated for 4 h with 1 mg/mL MTT solution. In the end, the MTT solution was washed, and the formazan crystals formed in the metabolically active cells were dissolved using isopropanol. The absorbance of the resulting solutions was determined at 550 nm using FlexStation III multimodal reader (Molecular Devices, San Jose, CA, USA). Untreated samples were prepared as controls.

Fluorescence Microscopy Assay

To investigate cells morphology under exposure to pristine and doxorubicin-loaded PNIPAM/mag NPs, MCF7 cells were seeded in 12-well plates at an initial density of 104 cells/cm² and after 24 h were exposed for one day to 100 µg/mL NPs. The monolayers were washed with PBS and fixed for 20 min with paraformaldehyde (PFA) 4% at 24 h of treatment. The cell membranes were then permeabilized for 30 min with a solution of bovine serum albumin (BSA) 2% and Triton × 100 (0.1%), and the cytoskeleton's actin filaments were stained for 1 h and 30 min at 37 °C and in darkness with a solution of Phalloidin-FITC. In the end, the staining solution was discarded, and the cell nuclei were

stained for 10 min with DAPI solution. An untreated monolayer was prepared similarly and served as control. All the samples were investigated by fluorescence microscopy using an Olympus IX73 inverted microscope with epifluorescence modulus (Olympus, Tokyo, Japan), and images were captured and processed using CellSense F software, version 1.11.

Statistical Analysis

The graphical representation of the obtained results was performed using the Graph-Pad Prism software, version 5.0. The mean of the obtained data was obtained from three independent experiments and is presented as the arithmetic mean S.D. The statistical significance (* $p < 0.05$) was determined using two-way ANOVA algorithm with Bonferroni test for group comparison.

3. Results

3.1. XRD and TEM for Magnetite Nanoparticles

X-ray diffractogram for a powder specimen of magnetic nanoparticles (MNPs) is shown in Figure 1. The indexed diffraction maxima correspond to Fe_3O_4 (ICDD 01-072-8149 file), the only phase in magnetite samples: 1.3° , 30.1° , 35.5° ; 43.1° , 53.4° , 57.1° , and 62.6° , corresponding to interplanar distances of 4.85 Å, 2.97 Å, 2.53 Å, 2.10 Å, 1.72 Å, 1.62 Å, and 1.48 Å and Miller indexes (111), (220), (311), (400), (422), (511), and (440). The as-prepared and indexed Fe_3O_4 compound has a face-centered cubic crystalline lattice with a lattice parameter $a = 8.394$ Å and a main diffraction maximum at Bragg angle 2θ of 35.44° . This corresponds to the Miller indices (311) with an interplanar distance of 2.53 Å and an average crystallite size of 7.3 nm (Scherrer formula). Bright-field TEM images in Figure 1A show the morphological features of magnetite nanoparticles with round and almost spherical shapes and sizes between 5 and 12 nm (agglomerates). Figure 1C reveals nanoparticle sizes of 6–9 nm with a relatively narrow distribution. The energy-dispersive X-ray analysis (Figure 1D) shows iron and oxygen as major elements, a fact that confirms that the nanoparticles from the agglomerates are iron oxide.

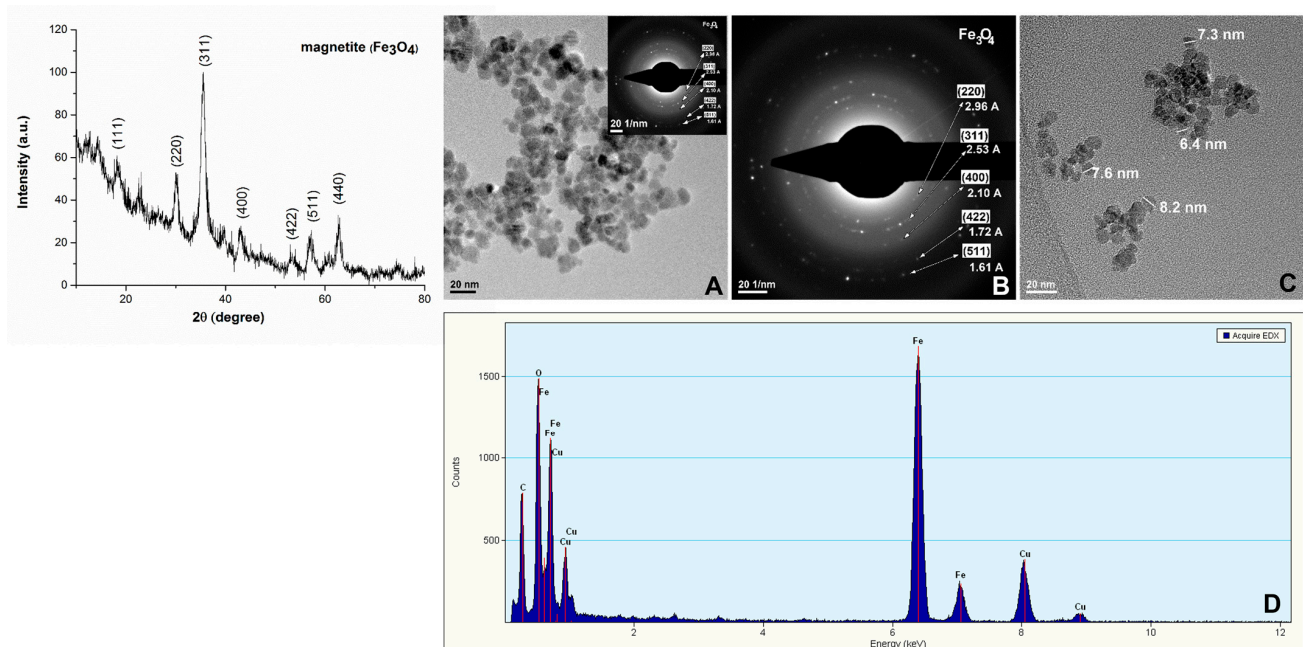


Figure 1. X-ray diffractogram and TEM characterization for magnetite nanoparticles: (A,C)—bright-field TEM images (BF-TEM); (B)—electron diffraction (SAED); (D)—Energy-dispersive X-ray analysis (EDAX).

3.2. Morphological Investigation (SEM)

The morphological investigation revealed similar characteristics between PNIPAM/magnetite nanoparticles with polymer solution concentrations ranging from 0.25 to 4%. SEM images showed the formation of nanoparticles only from 0.25% polymer concentration at three different temperatures (30 °C, 34 °C, and 38 °C). Figure 2 reveals PNIPAM/magnetite nanoparticles with a narrow size distribution, round shape, and also some agglomerates. Nanoparticles with sizes ranging between 50 and 200 nm were observed for all three nanoprecipitation temperatures. The individual nanoparticles reveal sizes below 100 nm, while the bigger shapes appear to be aggregates of several individual nanoparticles. The size distribution of nanoparticles is better shown in the corresponding histogram (Figure 3).

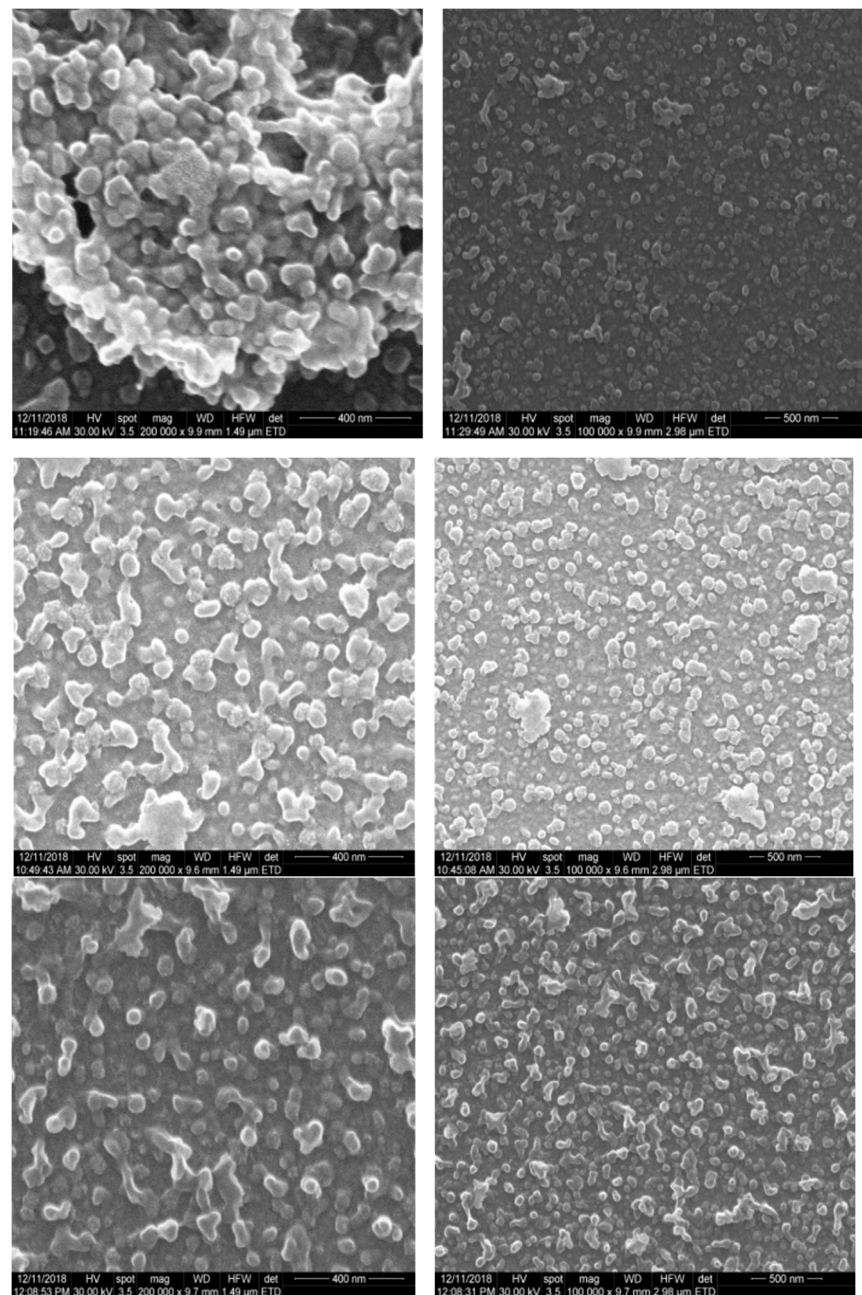


Figure 2. SEM images of PNIPAM/magnetite NPs at 30, 34, and 38 °C (0.25% PNIPAM solution).

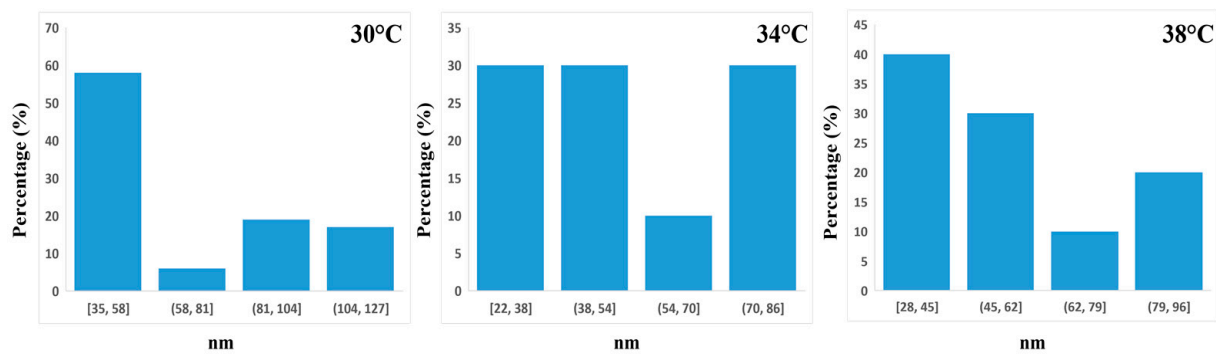


Figure 3. Histogram of size distributions of PNIPAM/magnetite NPs at various temperatures (0.25% PNIPAM solution).

3.3. Particle Size Measurements by Dynamic Light Scattering (DLS)

The evaluation of the PNIPAM/magnetite nanoparticle size distribution profile in solution was important to establish the main dimensional differences between the nanoparticles according to the preparation conditions. Poly(N-isopropylacrylamide) is a stimuli-responsive polymer that exhibits a reversible phase transition in aqueous solution (sol-gel) at 32–34 °C [46,47], called lower critical solution temperature (LCST). The three nanoprecipitation temperatures were chosen to act below the LCST (30 °C), near the LCST (34 °C), and above the LCST (38 °C). This approach could reveal the conformational behavior of PNIPAM chains within dual LCST and nanoprecipitation. The PNIPAM chains' spatial arrangement is of great importance to the nanoparticle size.

At 30 °C nanoprecipitation temperature (Table 2), DLS results revealed PNIPAM/magnetite nanoparticles with dimensions between 106 and 260 nm, depending on the polymer concentration. The increase in the polymer concentration led to an increase in the nanoparticle size. This behavior was previously observed in some research studies with other nanoparticles [48–50]. The results followed the same trend for 34 °C and 38 °C nanoprecipitation temperatures depending on the polymer concentration (Table 2). At the same polymer concentration and different nanoprecipitation temperatures, the nanoparticle size changes. Therefore, the smaller nanoparticle sizes were achieved at 34 °C for most polymer concentrations. This behavior was previously presented in the literature for PNIPAM/inorganic particle systems. The obtained results are in good agreement with the appropriate studies [51,52].

Table 2. Particle size of PNIPAM/magnetite nanoparticles by DLS.

Precipitation Temperature (°C)	Sample Name	Diameter, nm
30	PNIPAM 0.25%	106 ± 5
	PNIPAM 0.5%	112 ± 7
	PNIPAM 1%	141 ± 7
	PNIPAM 2%	190 ± 20
	PNIPAM 4%	260 ± 16
34	PNIPAM 0.25%	91 ± 3
	PNIPAM 0.5%	105 ± 5
	PNIPAM 1%	122 ± 15
	PNIPAM 2%	160 ± 15
	PNIPAM 4%	192 ± 18
38	PNIPAM 0.25%	102 ± 4
	PNIPAM 0.5%	114 ± 6
	PNIPAM 1%	124 ± 10
	PNIPAM 2%	155 ± 15
	PNIPAM 4%	172 ± 16

PNIPAM chains are water-soluble below the LCST due to the numerous hydrogen bonds between the polymer and water molecules. The nanoprecipitation involves the addition of polymer solution into acetone as a non-solvent. The water (solvent) and acetone (non-solvent) are miscible and allow the entrapment of water molecules within nanoparticles during preparation. Around the LCST, PNIPAM chains collapse towards a hydrophobic-like nature. This approach may be the main reason for the smaller size, as the water molecules are pulled out of the nanoparticles, resulting in a major volume shrinkage (Table 2). At temperatures above the LCST, the interaction between the polymer chains and water molecules leads to the breakage of the hydrogen bonds; therefore, the hydrophobic interaction between the hydrophobic moieties is strengthened while hydrogen bonding is simultaneously weakened. The thermodynamic size of the PNIPAM nanoparticles decreased gradually when the precipitation temperature was 34 and 38 °C since the polymer molecules became hydrophobic. Nanoprecipitation above the LCST occurs when the polymer chains probably start to relax and rearrange after collapsing. However, this process will not further allow the water molecules to penetrate the nanoparticle volume.

DLS results (Figure 4, Table 2) are correlated with SEM observations considering the size distribution pattern with respect to nanoprecipitation temperature and concentration. As for SEM analysis, the nanoparticles were dried and revealed smaller sizes in comparison with DLS data, where nanoparticle swelling occurred. Furthermore, DLS analysis provides dimensional results of the swollen nanoparticles together with the charging core around the nanoparticles' mass. Most probably, the sizes of the nanoparticles lie between SEM and DLS results.

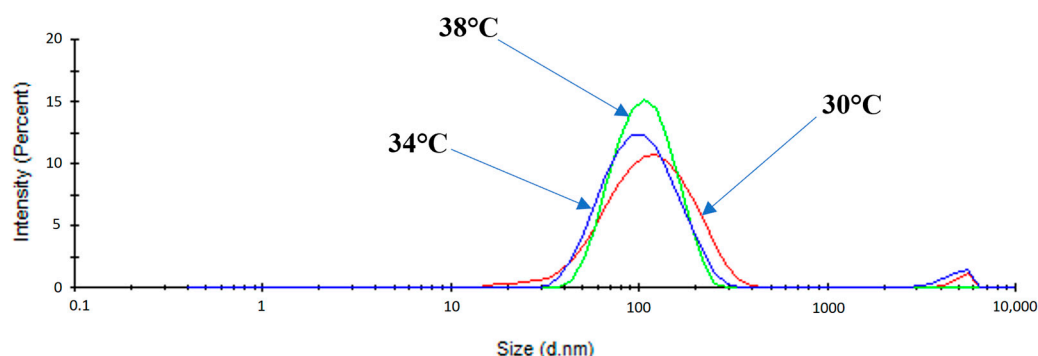


Figure 4. DLS investigation with nanoparticles' dimensional distribution at various nanoprecipitation temperatures.

3.4. Drug Release Behavior

Figure 5 shows the drug release curves for doxorubicin-loaded PNIPAM/magnetite nanoparticles prepared with different polymer concentrations. The release behavior for all nanoprecipitation temperatures (30, 34, and 38 °C) is presented. The drug release measurements were carried out in the same conditions for all samples: at neutral pH 7.45 and 37 °C. The increasing trend of the release efficiency with the PNIPAM concentration increase (0.25% to 4%) was observed. This trend can be correlated to the nanoparticle size, a higher size favoring a higher release efficiency. Additionally, it is important to note that the release efficiency (RE) for PNIPAM nanoparticles obtained at 30 °C is higher than those obtained at 34 and 38 °C (Table 3). This effect is attributed to the polymer collapsing chains around and above the LCST. Below the LCST, the polymer chains sustain the physical interactions with water molecules that entrap the nanoparticle volume. This fact favors the drug molecule release from the nanoparticles' mass.

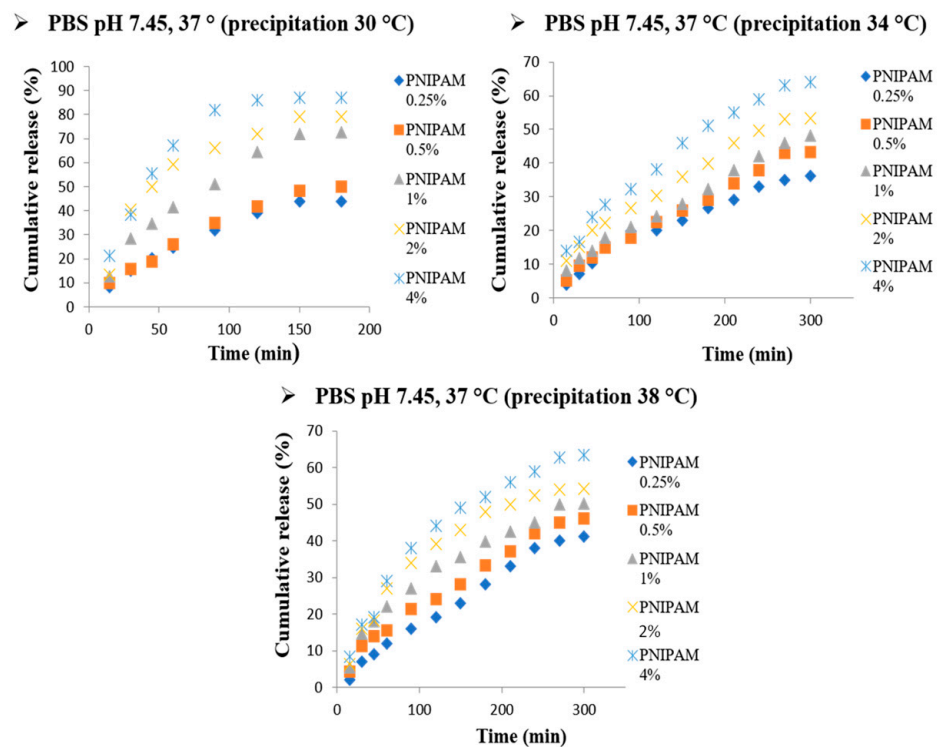


Figure 5. Doxorubicin release profiles from PNIPAM/magnetite nanoparticles in PBS at pH 7.45 and 37 °C (precipitation temperatures 30, 34, and 38 °C).

Table 3. Release efficiency of doxorubicin in PNIPAM/magnetite nanoparticles.

Precipitation Temperature (°C)	Sample Name	Release Efficiency (R.E. %)
30	PNIPAM 0.25%	43 ± 5
	PNIPAM 0.5%	49 ± 5
	PNIPAM 1%	70 ± 7
	PNIPAM 2%	79 ± 8
	PNIPAM 4%	87 ± 8
34	PNIPAM 0.25%	36 ± 5
	PNIPAM 0.5%	43 ± 5
	PNIPAM 1%	48 ± 5
	PNIPAM 2%	53 ± 5
	PNIPAM 4%	64 ± 6
38	PNIPAM 0.25%	41 ± 5
	PNIPAM 0.5%	46 ± 5
	PNIPAM 1%	50 ± 4
	PNIPAM 2%	54 ± 5
	PNIPAM 4%	63 ± 6

3.5. In Vitro Biological Results

3.5.1. PNIPAM/Magnetite NPs Biocompatibility Evaluation

The biocompatibility of the PNIPAM/magnetite NPs was evaluated in direct contact with the MCF7 breast cancer cells in order to validate their lack of toxicity and, consequently, their prospective use as drug delivery systems. For this, various dilutions of pristine PNIPAM/magnetite NPs ranging from 25 mg/mL to 50 µg/mL were applied on MCF7 monolayers for 24 h, and then the viability of the cells was evaluated by MTT assay and compared with the viability of untreated MCF7 cells. The obtained results are illustrated in Figure 6 and show that independent of the NPs dose, they did not impact the MCF7 cells' viability after 24 h of exposure in any way.

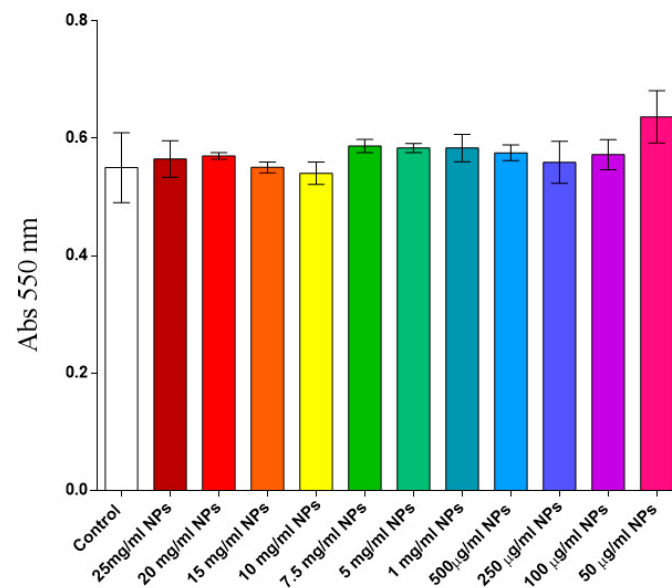


Figure 6. Graphical representation of MCF7 breast cancer cells viability after 24 h of treatment with pristine PNIPAM/magnetite NPs as shown by MTT assay (absorbance values at 550 nm).

Considering that the MCF7 cells' viability did not decrease by the exposure of the pristine PNIPAM/magnetite NPs, we concluded that the NPs are not cytotoxic on MCF7 cells and, therefore, were further used to encapsulate DOX for its controlled release in cancer cells.

3.5.2. DOX-Loaded PNIPAM/Magnetite NPs Working Dose

The IC₅₀ was determined for the DOX-loaded PNIPAM/magnetite NPs as a working dose for further in vitro investigations on MCF7 breast cancer cells. For this, various dilutions of DOX-loaded PNIPAM/magnetite NPs ranging from 25 mg/mL to 50 µg/mL were applied on MCF7 monolayers for 24 h. The cells' viability was then evaluated by MTT assay and compared with the viability of untreated cells. Our results are illustrated in Figure 7 and show that all the treatments significantly decreased cell viability as compared to an untreated sample.

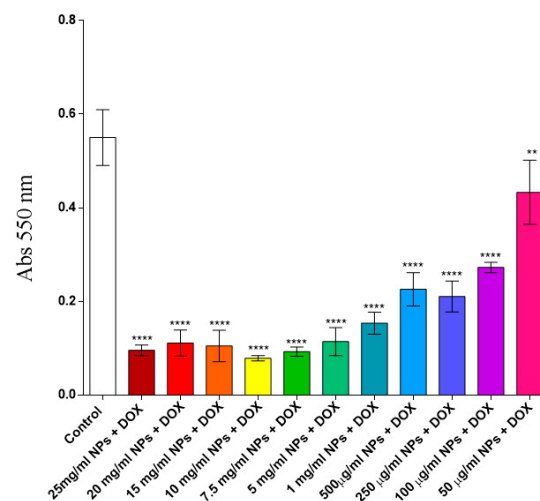


Figure 7. Graphical representation of MCF7 breast cancer cells viability after 24 h of treatment with DOX-loaded PNIPAM/magnetite NPs as shown by MTT assay (absorbance values at 550 nm); ** $p < 0.01$ 50 microg/mL NPs + DOX vs. control; **** $p < 0.0001$ 2 mg–100 microg/mL NPs + DOX vs. control.

Moreover, the DOX-loaded PNIPAM/magnetite NPs' potency in inhibiting MCF7 cells' viability was determined at a concentration of 100 $\mu\text{g}/\text{mL}$, and consequently, this dose was further used for the next *in vitro* investigations. Considering that the maximum amount of drug was found to be released after approx. 5 h, we decided to continue our experiments only after this minimum exposure, and therefore, all the *in vitro* studies on cell cultures were performed no earlier than 24 h of treatment.

3.5.3. DOX-Loaded PNIPAM/Magnetite NPs Potential to Alter MCF7 Cells Morphology

MCF7 breast cancer cell morphology was investigated after 24 h of treatment with pristine and DOX-loaded PNIPAM/magnetite NPs to find their potential to keep the actin filaments of the cytoskeleton similarly structured to those within the untreated cells. In this view, all the samples labeled with phalloidin-FITC and DAPI were inspected using an inverted Olympus IX73 microscope equipped with an epifluorescence modulus. The images captured after 24 h of treatment with 100 $\mu\text{g}/\text{mL}$ pristine and DOX-loaded PNIPAM/magnetite NPs were presented in Figure 8 and show that the untreated cells and the cells treated with pristine PNIPAM/magnetite NPs display a similar cytoskeleton organization, with well-defined and distributed actin filaments. In opposition, the images captured in the samples treated with DOX-loaded PNIPAM/magnetite NPs show that the cells display a very different shape and lack a homogenous expression of the actin filaments within the cytoplasm.

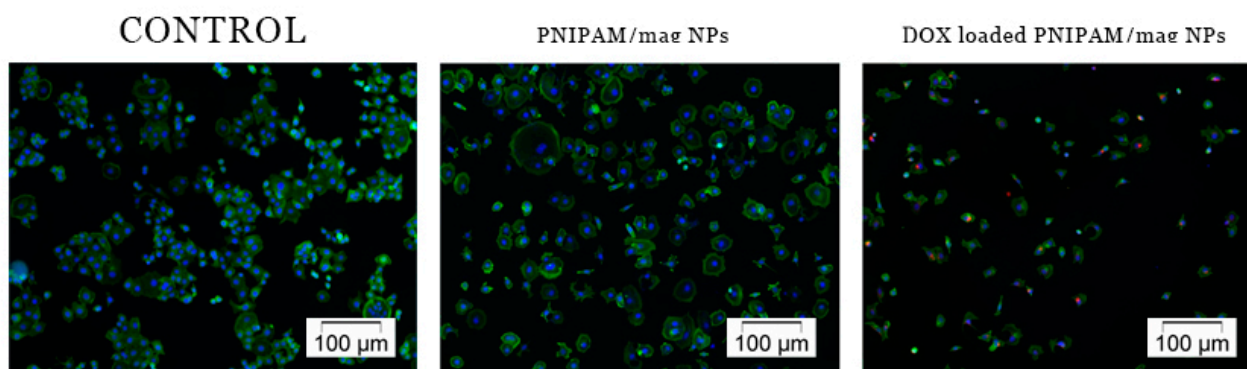


Figure 8. Fluorescence microscopy images of untreated MCF7 cells and MCF7 cells treated with pristine and DOX-loaded PNIPAM/magnetite NPs for 24 h and stained with phalloidin-FITC (green fluorescence—actin filaments) and DAPI (blue fluorescence—cells nuclei).

Moreover, these pictures resulting from merging the fluorescence channels display small dots of red fluorescence that can be explained only by the presence of NP aggregates containing DOX, known to have a bright red autofluorescence. Interestingly, these red fluorescence spots overlap the cells' shapes, indicating the MCF7 cells' potential to uptake the drug-loaded NPs. Consequently, the actin filaments of the MCF7 cells treated with DOX-loaded PNIPAM/magnetite NPs seem to not be able to assemble into a normal cytoskeleton, most probably due to the cytotoxic effect of the incorporated treatment.

4. Conclusions

The release behavior, morphology, and size distribution of thermosensitive PNIPAM/magnetite nanoparticles can be controlled by the process parameters, such as polymer solution concentration or nanoprecipitation temperature. Process control over nanoparticle features is important when developing nanoparticles for targeted applications. The hybrid nanoparticles are distributed more uniformly when they are prepared at temperatures around and above the LCST (34–38 $^{\circ}\text{C}$) due to the volume shrinkage and water molecules expulsion. The doxorubicin release behavior correlates with the nanoparticles' size distribution when polymer concentration is the main control parameter. Furthermore, the thermosensitive approach influences both nanoparticle features and release behavior when

nanoprecipitation temperature is the main control parameter. The biological assessment revealed that doxorubicin-loaded nanoparticles displayed a significant activity over MCF7 cell viability and cytoskeleton organization, while pristine nanoparticles displayed good biocompatibility with these cells. The nanoparticle size and release behavior play a vital role in anti-cancer activity. The reduced size increases the cancer cells' uptake potential, while the release behavior contributes to doxorubicin accumulation inside cancer cells. In conclusion, the characteristics of the nanoparticles can be optimized through the nanoprecipitation parameters to develop these nanocarriers for cancer management. The results revealed that the PNIPAM/magnetite drug-loaded systems can be used for a future study that includes radiation therapy potential. The uptake potential within MCF7 cancer cells is relevant for a complex biological assessment where a dual approach can be presented: anti-cancer chemotherapy and magnetic hyperthermia as synergistic effect.

Author Contributions: Conceptualization, C.Z., I.-C.R. and B.G.; methodology, I.-C.R., B.G. and C.Z.; validation, I.-C.R., B.G. and C.Z.; formal analysis, A.-C.I.M. and I.-C.R.; investigation, I.-C.R., A.-C.I.M., A.H., B.G. and E.T.; writing—original draft preparation, A.-C.I.M. and I.-C.R.; writing—review and editing, C.Z., B.G. and H.I.; supervision, C.Z. and H.I.; funding acquisition, I.-C.R. All authors have read and agreed to the published version of the manuscript.

Funding: This work was supported by a grant of the Ministry of Research, Innovation and Digitization, CNCS-UEFISCDI, project number PN-III-P1-1.1-PD-2021-0478, within PNCDI III.

Data Availability Statement: The data presented in this study are available on request from the corresponding author.

Acknowledgments: This work has been supported by the European Social Fund from the Sectoral Operational Programme Human Capital 2014–2020 through the Financial Agreement with the title “Training of PhD students and postdoctoral researchers in order to acquire applied research skills-SMART”, Contract no. 13530/16.06.2022-SMIS code: 153734. DLS was possible due to European Regional Development Fund through Competitiveness Operational Program 2014–2020, priority axis 1, Project No. P_36_611, MySMIS code 107066, Innovative Technologies for Materials Quality Assurance in Health, Energy and Environmental—Center for Innovative Manufacturing Solutions of Smart Biomaterials and Biomedical Surfaces—INOVABIOMED.

Conflicts of Interest: The authors declare no conflict of interest. The funders had no role in the design of this study; in the collection, analyses, or interpretation of data; in the writing of the manuscript; or in the decision to publish the results.

References

1. Ferlay, J.; Colombet, M.; Soerjomataram, I.; Parkin, D.M.; Piñeros, M.; Znaor, A.; Bray, F. Cancer statistics for the year 2020: An overview. *Int. J. Cancer* **2021**, *149*, 778–789. [[CrossRef](#)]
2. Arnold, M.; Morgan, E.; Runggay, H.; Mafra, A.; Singh, D.; Laversanne, M.; Vignat, J.; Gralow, J.R.; Cardoso, F.; Siesling, S.; et al. Current and future burden of breast cancer: Global statistics for 2020 and 2040. *Breast* **2022**, *66*, 15–23. [[CrossRef](#)] [[PubMed](#)]
3. Wilkinson, L.; Gathani, T. Understanding breast cancer as a global health concern. *Br. J. Radiol.* **2022**, *95*, 20211033. [[CrossRef](#)]
4. Giaquinto, A.N.; Sung, H.; Miller, K.D.; Kramer, J.L.; Newman, L.A.; Minihan, A.; Jemal, A.; Siegel, R.L. Breast Cancer Statistics, 2022. *CA Cancer J. Clin.* **2022**, *72*, 524–541. [[CrossRef](#)]
5. Siegel, R.L.; Miller, K.D.; Fuchs, H.E.; Jemal, A. Cancer statistics, 2022. *CA Cancer J. Clin.* **2022**, *72*, 7–33. [[CrossRef](#)]
6. Bahreyni, A.; Mohamud, Y.; Luo, H. Emerging nanomedicines for effective breast cancer immunotherapy. *J. Nanobiotechnol.* **2020**, *18*, 180. [[CrossRef](#)]
7. Thun, M.J.; DeLancey, J.O.; Center, M.M.; Jemal, A.; Ward, E.M. The global burden of cancer: Priorities for prevention. *Carcinogenesis* **2010**, *31*, 100–110. [[CrossRef](#)]
8. Rodrigues, M. Five young investigators tackle big questions in oncology. *Nat. Med.* **2022**, *28*, 630–632. [[CrossRef](#)] [[PubMed](#)]
9. Luo, L.; Xu, F.; Peng, H.; Luo, Y.; Tian, X.; Battaglia, G.; Zhang, H.; Gong, Q.; Gu, Z.; Luo, K. Stimuli-responsive polymeric prodrug-based nanomedicine delivering nifuroxazide and doxorubicin against primary breast cancer and pulmonary metastasis. *J. Control. Release* **2020**, *318*, 124–135. [[CrossRef](#)] [[PubMed](#)]
10. Yang, S.X.; Hewitt, S.M.; Yu, J. Locoregional tumor burden and risk of mortality in metastatic breast cancer. *npj Precis. Oncol.* **2022**, *6*, 22. [[CrossRef](#)]
11. Wang, L.; Zhang, S.; Wang, X. The Metabolic Mechanisms of Breast Cancer Metastasis. *Front. Oncol.* **2021**, *10*, 602416. [[CrossRef](#)]

12. Azamjah, N.; Soltan-Zadeh, Y.; Zayeri, F. Global Trend of Breast Cancer Mortality Rate: A 25-Year Study. *Asian Pac. J. Cancer Prev.* **2019**, *20*, 2015–2020. [[CrossRef](#)] [[PubMed](#)]
13. Chan, S.; Friedrichs, K.; Noel, D.; Pintér, T.; Van Belle, S.; Vorobiof, D.; Duarte, R.; Gil Gil, M.; Bodrogi, I.; Murray, E.; et al. Prospective randomized trial of docetaxel versus doxorubicin in patients with metastatic breast cancer. *J. Clin. Oncol.* **1999**, *17*, 2341–2354. [[CrossRef](#)]
14. Shafei, A.; El-Bakly, W.; Sobhy, A.; Wagdy, O.; Reda, A.; Aboelenin, O.; Marzouk, A.; El Habak, K.; Mostafa, R.; Ali, M.A.; et al. A review on the efficacy and toxicity of different doxorubicin nanoparticles for targeted therapy in metastatic breast cancer. *Biomed Pharm.* **2017**, *95*, 1209–1218. [[CrossRef](#)]
15. Edwardson, D.W.; Narendrula, R.; Chewchuk, S.; Mispel-Beyer, K.; Mapletoft, J.P.; Parissenti, A.M. Role of Drug Metabolism in the Cytotoxicity and Clinical Efficacy of Anthracyclines. *Curr. Drug Metab.* **2015**, *16*, 412–426. [[CrossRef](#)]
16. Al-malky, H.S.; Al Harthi, S.E.; Osman, A.-M.M. Major obstacles to doxorubicin therapy: Cardiotoxicity and drug resistance. *J. Oncol. Pharm. Pract.* **2020**, *26*, 434–444. [[CrossRef](#)]
17. Su, Y.; Xie, Z.; Kim, G.B.; Dong, C.; Yang, J. Design Strategies and Applications of Circulating Cell-Mediated Drug Delivery Systems. *ACS Biomater. Sci. Eng.* **2015**, *1*, 201–217. [[CrossRef](#)]
18. Grund, S.; Bauer, M.; Fischer, D. Polymers in Drug Delivery—State of the Art and Future Trends. *Adv. Eng. Mater.* **2011**, *13*, B61–B87. [[CrossRef](#)]
19. Pillai, O.; Panchagnula, R. Polymers in drug delivery. *Curr. Opin. Chem. Biol.* **2001**, *5*, 447–451. [[CrossRef](#)] [[PubMed](#)]
20. Tong, R.; Langer, R. Nanomedicines Targeting the Tumor Microenvironment. *Cancer J.* **2015**, *21*, 314–321. [[CrossRef](#)]
21. Luo, X.; Zhang, Q.; Chen, H.; Hou, K.; Zeng, N.; Wu, Y. Smart Nanoparticles for Breast Cancer Treatment Based on the Tumor Microenvironment. *Front. Oncol.* **2022**, *12*, 907684. [[CrossRef](#)]
22. Liu, D.; Yang, F.; Xiong, F.; Gu, N. The Smart Drug Delivery System and Its Clinical Potential. *Theranostics* **2016**, *6*, 1306–1323. [[CrossRef](#)] [[PubMed](#)]
23. Brigger, I.; Dubernet, C.; Couvreur, P. Nanoparticles in cancer therapy and diagnosis. *Adv. Drug Deliv. Rev.* **2002**, *54*, 631–651. [[CrossRef](#)]
24. Tiwari, G.; Tiwari, R.; Sriwastawa, B.; Bhati, L.; Pandey, S.; Pandey, P.; Bannerjee, S.K. Drug delivery systems: An updated review. *Int. J. Pharm. Investig.* **2012**, *2*, 2–11. [[CrossRef](#)]
25. Hou, K.; Ning, Z.; Chen, H.; Wu, Y. Nanomaterial Technology and Triple Negative Breast Cancer. *Front. Oncol.* **2021**, *11*, 828810. [[CrossRef](#)]
26. Kashyap, S.; Singh, N.; Surnar, B.; Jayakannan, M. Enzyme and Thermal Dual Responsive Amphiphilic Polymer Core-Shell Nanoparticle for Doxorubicin Delivery to Cancer Cells. *Biomacromolecules* **2016**, *17*, 384–398. [[CrossRef](#)]
27. Rao, N.V.; Ko, H.; Lee, J.; Park, J.H. Recent Progress and Advances in Stimuli-Responsive Polymers for Cancer Therapy. *Front. Bioeng. Biotechnol.* **2018**, *6*, 110. [[CrossRef](#)]
28. Wu, M.; Huang, S. Magnetic nanoparticles in cancer diagnosis, drug delivery and treatment. *Mol. Clin. Oncol.* **2017**, *7*, 738–746. [[CrossRef](#)]
29. Farzin, A.; Etesami, S.A.; Quint, J.; Memic, A.; Tamayol, A. Magnetic Nanoparticles in Cancer Therapy and Diagnosis. *Adv. Healthc. Mater.* **2020**, *9*, 1901058. [[CrossRef](#)]
30. Fathi Karkan, S.; Mohammadhosseini, M.; Panahi, Y.; Milani, M.; Zarghami, N.; Akbarzadeh, A.; Abasi, E.; Hosseini, A.; Davaran, S. Magnetic nanoparticles in cancer diagnosis and treatment: A review. *Artif. Cells Nanomed. Biotechnol.* **2017**, *45*, 1–5. [[CrossRef](#)] [[PubMed](#)]
31. Liu, R.; Fraylich, M.; Saunders, B.R. Thermoresponsive copolymers: From fundamental studies to applications. *Colloid Polym. Sci.* **2009**, *287*, 627–643. [[CrossRef](#)]
32. Hoffman, A.S. “Intelligent” Polymers in Medicine and Biotechnology. *Artif. Organs* **1995**, *19*, 458–467. [[CrossRef](#)]
33. Heskins, M.; Guillet, J.E. Solution Properties of Poly(N-isopropylacrylamide). *J. Macromol. Sci. Part A Chem.* **1968**, *2*, 1441–1455. [[CrossRef](#)]
34. Gupta, S.; Singh, A.; Matsumi, N. Controlled Phase Behavior of Thermally Sensitive Poly(N-isopropylacrylamide/ionic liquid) with Embedded Au Nanoparticles. *ACS Omega* **2019**, *4*, 20923–20930. [[CrossRef](#)]
35. Zheng, Y.; Wang, L.; Lu, L.; Wang, Q.; Benicewicz, B.C. pH and Thermal Dual-Responsive Nanoparticles for Controlled Drug Delivery with High Loading Content. *ACS Omega* **2017**, *2*, 3399–3405. [[CrossRef](#)]
36. Radu, I.-C.; Biru, I.-E.; Damian, C.-M.; Ion, A.-C.; Iovu, H.; Tanasa, E.; Zaharia, C.; Galateanu, B. Grafting versus Crosslinking of Silk Fibroin-g-PNIPAM via Tyrosine-NIPAM Bridges. *Molecules* **2019**, *24*, 4096. [[CrossRef](#)]
37. Stănescu, P.O.; Radu, I.C.; Drăghici, C.; Teodorescu, M. Controlling the thermal response of poly(N-isopropylacrylamide)-poly(ethylene glycol)-poly(N-isopropylacrylamide) triblock copolymers in aqueous solution by means of additives. *React. Funct. Polym.* **2020**, *152*, 104610. [[CrossRef](#)]
38. Namgung, H.; Jo, S.; Lee, T.S. Fluorescence Modulation of Conjugated Polymer Nanoparticles Embedded in Poly(N-Isopropylacrylamide) Hydrogel. *Polymers* **2021**, *13*, 4315. [[CrossRef](#)]
39. Nowaczyk, M.; Zimna, A.; Deptuła, T.; Fiedorowicz, K.; Rozwadowska, N.; Podralska, M.; Kurpisz, M. pNiPAM-Nanoparticle-Based Antiapoptotic Approach for Pro-Regenerative Capacity of Skeletal Myogenic Cells. *Nanomaterials* **2021**, *11*, 2495. [[CrossRef](#)]
40. Cui, G.; Wang, H.; Long, S.; Zhang, T.; Guo, X.; Chen, S.; Kakuchi, T.; Duan, Q.; Zhao, D. Thermo- and Light-Responsive Polymer-Coated Magnetic Nanoparticles as Potential Drug Carriers. *Front. Bioeng. Biotechnol.* **2022**, *10*, 931830. [[CrossRef](#)]

41. Karg, M.; Hellweg, T. New “smart” poly(NIPAM) microgels and nanoparticle microgel hybrids: Properties and advances in characterisation. *Curr. Opin. Colloid Interface Sci.* **2009**, *14*, 438–450. [[CrossRef](#)]
42. Yar, Y.; Khodadust, R.; Akkoc, Y.; Utkur, M.; Saritas, E.U.; Gozuacik, D.; Yagci Acar, H. Development of tailored SPION-PNIPAM nanoparticles by ATRP for dually responsive doxorubicin delivery and MR imaging. *J. Mater. Chem. B* **2018**, *6*, 289–300. [[CrossRef](#)]
43. Witt, M.U.; Hinrichs, S.; Möller, N.; Backes, S.; Fischer, B.; von Klitzing, R. Distribution of CoFe₂O₄ Nanoparticles Inside PNIPAM-Based Microgels of Different Cross-linker Distributions. *J. Phys. Chem. B* **2019**, *123*, 2405–2413. [[CrossRef](#)] [[PubMed](#)]
44. Garcia-Pinel, B.; Ortega-Rodríguez, A.; Porrás-Alcalá, C.; Cabeza, L.; Contreras-Cáceres, R.; Ortiz, R.; Díaz, A.; Moscoso, A.; Sarabia, F.; Prados, J.; et al. Magnetically active pNIPAM nanosystems as temperature-sensitive biocompatible structures for controlled drug delivery. *Artif. Cells Nanomed. Biotechnol.* **2020**, *48*, 1022–1035. [[CrossRef](#)]
45. Reis, C.P.; Neufeld, R.J.; Ribeiro, A.J.; Veiga, F.; Nanoencapsulation, I. Methods for preparation of drug-loaded polymeric nanoparticles. *Nanomedicine* **2006**, *2*, 8–21. [[CrossRef](#)]
46. Jain, K.; Vedarajan, R.; Watanabe, M.; Ishikiriya, M.; Matsumi, N. Tunable LCST behavior of poly(N-isopropylacrylamide/ionic liquid) copolymers. *Polym. Chem.* **2015**, *6*, 6819–6825. [[CrossRef](#)]
47. Jones, S.T.; Walsh-Korb, Z.; Barrow, S.J.; Henderson, S.L.; del Barrio, J.; Scherman, O.A. The Importance of Excess Poly(N-isopropylacrylamide) for the Aggregation of Poly(N-isopropylacrylamide)-Coated Gold Nanoparticles. *ACS Nano* **2016**, *10*, 3158–3165. [[CrossRef](#)]
48. Radu, I.-C.; Hudita, A.; Zaharia, C.; Stanescu, P.O.; Vasile, E.; Iovu, H.; Stan, M.; Ginghina, O.; Galateanu, B.; Costache, M.; et al. Poly(HydroxyButyrate-co-HydroxyValerate) (PHBHV) Nanocarriers for Silymarin Release as Adjuvant Therapy in Colo-rectal Cancer. *Front. Pharmacol.* **2017**, *8*, 508. [[CrossRef](#)]
49. Stanescu, P.-O.; Radu, I.-C.; Leu Alexa, R.; Hudita, A.; Tanasa, E.; Ghitman, J.; Stoian, O.; Tsatsakis, A.; Ginghina, O.; Zaharia, C.; et al. Novel chitosan and bacterial cellulose biocomposites tailored with polymeric nanoparticles for modern wound dressing development. *Drug Deliv.* **2021**, *28*, 1932–1950. [[CrossRef](#)]
50. Radu, I.C.; Hudita, A.; Zaharia, C.; Galateanu, B.; Iovu, H.; Tanasa, E.; Georgiana Nitu, S.; Ginghina, O.; Negrei, C.; Tsatsakis, A.; et al. Poly(3-hydroxybutyrate-CO-3-hydroxyvalerate) PHBHV biocompatible nanocarriers for 5-FU delivery targeting colorectal cancer. *Drug Deliv.* **2019**, *26*, 318–327. [[CrossRef](#)] [[PubMed](#)]
51. Chen, C.; Ng, D.Y.W.; Weil, T. Polymer-grafted gold nanoflowers with temperature-controlled catalytic features by in situ particle growth and polymerization. *Mater. Chem. Front.* **2019**, *3*, 1449–1453. [[CrossRef](#)]
52. Yeshchenko, O.A.; Naumenko, A.P.; Kutsevol, N.V.; Maskova, D.O.; Harahuts, I.I.; Chumachenko, V.A.; Marinin, A.I. Anomalous Inverse Hysteresis of Phase Transition in Thermosensitive Dextran-graft-PNIPAM Copolymer / Au Nanoparticles Hybrid Nanosystem. *J. Phys. Chem. C* **2018**, *122*, 8003–8010. [[CrossRef](#)]

Disclaimer/Publisher’s Note: The statements, opinions and data contained in all publications are solely those of the individual author(s) and contributor(s) and not of MDPI and/or the editor(s). MDPI and/or the editor(s) disclaim responsibility for any injury to people or property resulting from any ideas, methods, instructions or products referred to in the content.